Journal of Alloys and Compounds 509 (2011) 7844–7853

Contents lists available at ScienceDirect

Journal of Alloys and Compounds

journal homepage: www.elsevier.com/locate/jallcom

Review

Li–Mg–N–H-based combination systems for hydrogen storage

Chu Liang, Yongfeng Liu*, Hongliang Fu, Yufan Ding, Mingxia Gao, Hongge Pan

State Key Laboratory of Silicon Materials & Department of Materials Science and Engineering, Zhejiang University, 38 Zheda Road, Hangzhou 310027, People's Republic of China

ARTICLE INFO

Article history:
Received 17 February 2011
Received in revised form 21 April 2011
Accepted 22 April 2011
Available online 14 May 2011

Keywords:
Hydrogen storage materials
Metal–N–H-based materials
Thermodynamics
Kinetics
Reaction mechanisms

ABSTRACT

Metal–N–H-based materials are of particular interest as a group of new complex hydrides owing to their potential applications in hydrogen storage. A variety of metal–N–H-based systems have been developed so far for their hydrogen storage performances. This review deals with the Li–Mg–N–H-based combination systems which are widely recognized as one of the most promising hydrogen storage media for practical applications. The emphasis is on the structural characteristics of the lithium/magnesium amides/imides/nitrides, the hydrogen storage properties determined by the material compositions, the thermodynamics and kinetics of the hydrogen storage process, and the reaction mechanisms for de-/hydrogenation of the Li–Mg–N–H combination systems. The challenges and direction in further improving the hydrogen storage performances of the Li–Mg–N–H-based combination systems are pointed out as well.

Contents

1. Introduction

The rapidly dwindling of fossil fuel resources (especially petroleum and natural gas) coupled with the growing environmental concerns has brought increasing awareness of the need for efficient, clean and renewable energy sources, especially for mobile applications [1,2]. Hydrogen is an energy carrier which is transportable, storable and convertible, and has a big potential to become the ultimate solution to energy security, resource availability, and environmental compatibility [3–5]. However, the greatest challenge in the development of hydrogen-based technologies is to store hydrogen safely, effectively and economically [6–8].

Hydrogen storage plays a critical bridge role in connecting hydrogen production with hydrogen applications [9]. At standard temperature and pressure (STP), hydrogen is a gas with density of 0.08988 g L^{-1}. As a result, the volumetric storage density of hydrogen gas is too low for practical purpose, especially for the use in transportation. To achieve the widespread commercialization, the

* Corresponding author. Tel.: +86 571 87952615; fax: +86 571 87952615.
E-mail address: mselyf@zju.edu.cn (Y. Liu).

0925-8388/$ – see front matter © 2011 Elsevier B.V. All rights reserved.
doi:10.1016/j.jallcom.2011.04.123

Table 1
DOE targets for onboard hydrogen storage systems for light-duty vehicles [13].

Storage parameter	Units	Old targets		New targets		
		2010	2015	2010	2015	Ultimate
System gravimetric capacity	wt%	4.5	6	4.5	5.5	7.5
	(kWh kg^{-1})	(1.5)	(2.0)	(1.5)	(1.8)	(2.5)
System volumetric capacity	g L^{-1}	28	45	28	40	70
	kWh L^{-1}	0.9	1.5	0.9	1.3	2.3
Min/max delivery temperature	°C	−40/85	−40/85	−40/85	−40/85	−40/95–105
Min/max delivery pressure from storage system	bar (abs)	4/10	3/10	5/12	5/12	3/12
Operational cycle life (1/4 tank to full)	cycles	1500	1500	1000	1500	1500
System fill time (for 5 kg H_2)	min	3	2.5	4.2	3.3	2.5
	(kg H_2 min^{-1})	(1.7)	(2.0)	(1.2)	(1.5)	(2.0)
Minimum full flow rate	g s^{-1} kW^{-1}	0.02	0.02	0.02	0.02	0.02
Storage system cost	$ kWh^{-1} net	4	2	To be determined		

performance of hydrogen-fueled vehicles must be comparable or superior to conventional gasoline vehicles. At the heart of the issue is that a hydrogen storage technology allows a driving range of more than 300 miles (500 km) without making significant changes to the vehicle and being available at similar cost. By translating vehicle performance requirements into storage system needs, the U.S. Department of Energy (DOE) initially established a series of technical targets (Table 1) in 2003 to guide efforts in developing on-board hydrogen storage systems for vehicle applications [10]. However, the original DOE targets were formulated only by comparing the performance of a fuel cell vehicle (FCV) to an advanced gasoline internal combustion engine (ICE) vehicle as the baseline since very little FCV data was available at that time. Since then, significant progress has been made on the development of hydrogen fuelled vehicles [11]. Moreover, "Real-world" driving and testing experience has been accumulated and valuable information has been substantially gathered through understanding fuel cell vehicle system design limitations, vehicle performance, and customer requirements and expectations [12]. As a result of these new developments, the DOE has updated the technical targets for on-board hydrogen storage systems in 2009 [13]. As shown in Table 1, the new 2015 targets are reduced to 5.5 wt% for gravimetric hydrogen density and 40 g H_2 L^{-1} for volumetric hydrogen density. At the same time, a new "Ultimate Full Fleet" target was put forward to be 7.5 wt% for gravimetric hydrogen density and 70 g H_2 L^{-1} for volumetric hydrogen density. While the "Ultimate Full Fleet" targets represent a ~17% and 14% decrease in gravimetric and volumetric hydrogen density, respectively, relative to the previous 2015 target, they have a similar meaning in that both sets of targets were designed to travel greater than 300 miles on a single hydrogen fill.

With respect to the chemical nature of hydrogen, materials-based solid-state hydrogen storage by adsorption on materials with high specific area or chemically bonded in covalent and ionic compounds is extensively believed to be a practically viable ultimate solution from a safety perspective [2,7–9,14]. Scientific interest in materials-based hydrogen storage was originated from the fact that hydrogen can reacts with many metallic elements and alloys to form a range of metal hydrides in which hydrogen can be readily released [15,16]. Over the years a number of hydrogen storage materials have been designed and developed for their hydrogen storage performances. Investigations have expanded beyond the conventional metal hydrides to the complex hydrides [17–28]. The typical complex hydrides are composed of light metal cations (mainly including alkali or alkaline earth metals Li, Na, Mg, Ca, etc.) and hydrogen-containing anion complex in which hydrogen atoms are covalently bonded to central atoms, such as B, Al or N [27]. Among them, the metal–N–H-based combination systems have attracted considerable attention since Chen et al. reported that lithium nitride (Li_3N) could reversibly absorb/desorb ~11.4 wt% of hydrogen [28]. However, the temperature required to liberate hydrogen from the hydrogenated Li_3N is in excess of 250 °C, which is too high for on-board applications. To lower the operating temperatures, numerous efforts have been devoted to the thermodynamic destabilization of the Li–N–H system by replacing lithium with other alkali or alkaline earth metals, and a variety of new metal–N–H combination systems were synthesized and characterized, such as Li–Mg–N–H, Li–Ca–N–H, Li–Al–N–H, Mg–Ca–N–H, Li–B–N–H, and so on [29–36]. Excitingly enough, the Li–Mg–N–H combination system composed of $Mg(NH_2)_2$ and LiH exhibits moderate operating temperatures, good reversibility, and a relatively high hydrogen capacity of 5.6 wt% [29,30].

A number of reviews have already summarized progress made in hydrogen storage materials over the last decade [37–43]. These reviews usually cover the broad spectrum of materials ranging from metal hydrides, complex hydrides to porous materials. This review focuses on advances made with the Li–Mg–N–H combination system, one of the newly developed complex materials with high potential for on-board hydrogen storage applications. Special emphasis is given to the up-to-date knowledge about the correlation between the material compositions, structures and hydrogen storage properties. The review begins with a systematic summary of the preparation methods and structure characteristics of the relevant amides, imides and nitrides. The relationship between the hydrogen storage behaviors and the material compositions are discussed. The improved thermodynamics and kinetics for hydrogen storage process are highlighted. The reaction mechanisms proposed presently for hydrogen storage in the Li–Mg–N–H combination systems are emphasized. Finally, it concludes with some perspectives and outlook on the future developments of the Li–Mg–N–H-based hydrogen storage materials.

2. Synthesis and structures of lithium/magnesium amides, imides and nitrides

The introduction of nitrogen into the hydrogen storage systems expands the scope of material selection. Lithium/magnesium hydrides, amides, imides and nitrides are the major reactants for preparing the Li–Mg–N–H-based combination systems for hydrogen storages. Therefore, their preparation methods and structural characteristics correlate closely to the reaction activity for hydrogen storage applications.

2.1. Amides

Lithium amide ($LiNH_2$) was first synthesized in 1894 by Titherley [44]. The synthetic process of lithium amides can be described by the following reaction with an exothermic nature [45,46].

$$LiH + NH_3 \rightarrow LiNH_3 + H_2 \quad (1)$$

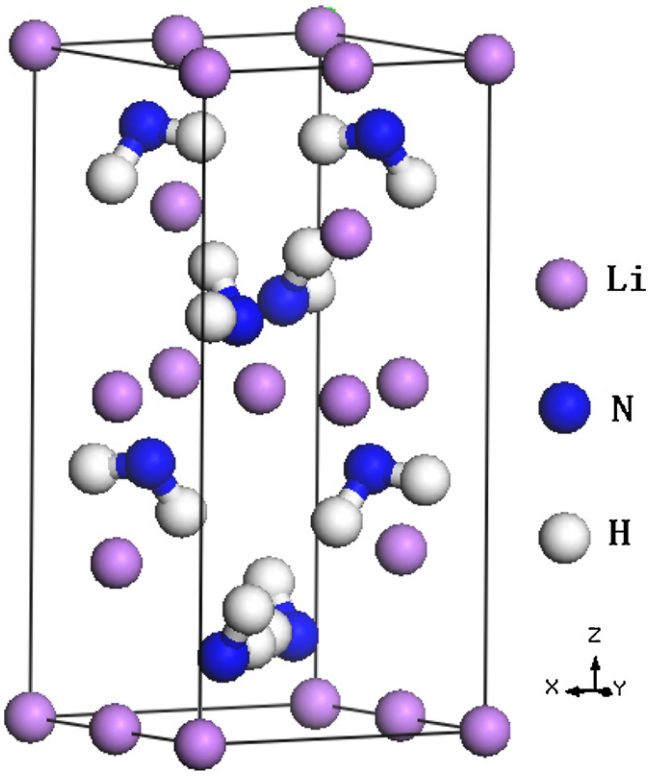

Fig. 1. Crystal structure of $LiNH_2$ [49].

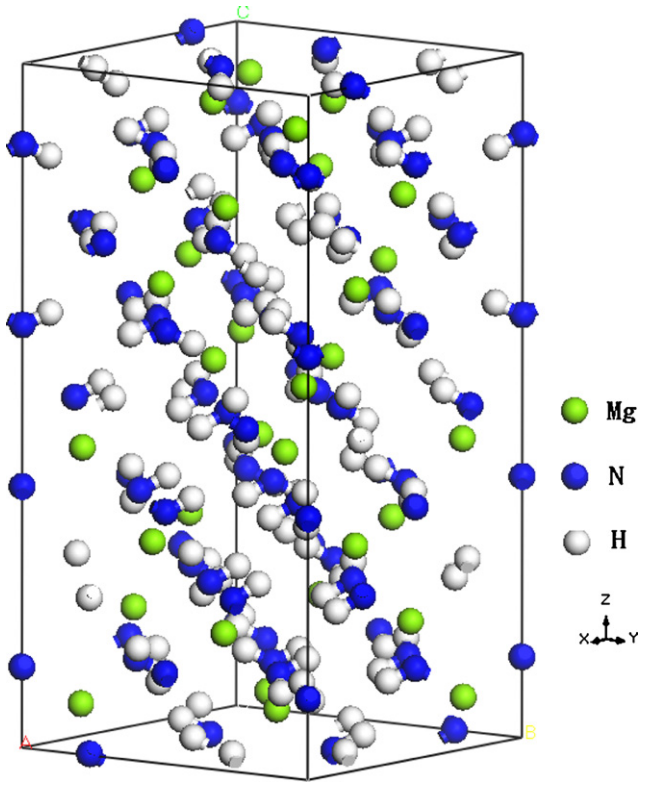

Fig. 2. Crystal structure of $Mg(NH_2)_2$ [57].

In comparison with conventional preparation methods by directly heating the pure metal or hydride under NH_3 atmosphere, ball milling hydrides under ammonia atmosphere is an alternative technique for preparing amides [46]. LiH can react completely with NH_3 within 2 h room temperature ball milling under the NH_3 atmosphere of 4 bar while the reaction extent is only about 1.5% as reacting LiH under 4 bar of NH_3 atmosphere within 3 h at 100 °C without any ball milling [46]. Recently, vacuum evaporation was employed to synthesize $LiNH_2$ films on the basis of the physical characteristics of low melting and high boiling temperatures of metallic Li [47,48]. Nakamori et al. [48] obtained the $LiNH_2$ films by means of vacuum evaporation of metallic Li on a Mo substrate at 600 °C followed by nitrogenation and hydrogenation at 220 °C under high-purity nitrogen and hydrogen gases, respectively. The crystal structure of $LiNH_2$ was determined to be a tetragonal structure (space group $I\bar{4}$) with lattice constants of $a = 5.03442$ Å and $c = 10.25558$ Å by means of power neutron diffraction [49]. Hydrogen atoms occupy the $8g_1$ and $8g_2$ sites, nitrogen atoms occupy the 8g sites, and lithium atoms occupy the 2a, 4f and 2c sites. As shown in Fig. 1, the lithium is tetrahedrally coordinated with four NH_2 groups [49]. The electronic structure analyses based on first-principles calculations show strong ionic characteristics between the Li^+ cation and the covalent bonded $[NH_2]^-$ anion [50]. The N–H bonds of lithium amides are infrared (IR) active, and the typical IR absorption peaks centered at 3312/3258, and 1561/1539 cm^{-1}, which are corresponding to N–H stretching vibration modes and H–N–H deformation vibration modes, respectively [51].

Magnesium amide ($Mg(NH_2)_2$) can be obtained by the solid–gas reactions of MgH_2, Mg or Mg_3N_2 with ammonia. However, the reaction of MgH_2 with NH_3 is sluggish with respect to the reaction between LiH and NH_3 [52]. It takes around 13 h to finish the reaction between MgH_2 and NH_3 at room temperature by means of ball milling, 2 h delay relative to LiH [46]. $Mg(NH_2)_2$ can also be produced by both heating MgH_2 to 330–380 °C under 5 bar ammonia atmosphere and milling MgH_2 under 5 bar ammonia atmosphere followed by annealing at 300 °C [53,54]. Additionally, a facile method for preparing $Mg(NH_2)_2$ is to react directly Mg powder with NH_3 at 300 °C as described by the following reaction [34,55].

$$Mg + 2NH_3 \rightarrow Mg(NH_2)_2 + H_2 \quad (2)$$

Recently, Xie et al. [56] prepared the hollow nanospheres of $Mg(NH_2)_2$ by reacting Mg_3N_2 nanotubes with NH_3 based on the Kirkendall effect, in which Mg_3N_2 nanotubes were first obtained by evaporating Mg metal in NH_3 atmosphere with plasma metal reaction. It is well known that $Mg(NH_2)_2$ is crystallized in a tetragonal structure ($I4_1/acd$) with lattice constants of $a = 10.3758$ Å and $c = 20.062$ Å [57]. Fig. 2 shows the crystal structure of $Mg(NH_2)_2$ determined by the neutron diffraction. It can be seen that the Mg^{2+} cation is tetrahedrally coordinated by four amide $[NH_2]^-$ anions [57,58]. The typical IR absorption peaks of N–H vibration modes and H–N–H deformation vibration modes of $Mg(NH_2)_2$ are centered at 3325, 3274 and 1572 cm^{-1}, respectively [55].

2.2. Imides

In general, metal amides can convert to their corresponding imides or nitrides through self-decomposition at elevated temperatures. For example, the lithium imide (Li_2NH) is produced as heating $LiNH_2$ to 230–450 °C [59]. Chen et al. [28] found that Li_2NH is also the dehydrogenation product of the $LiNH_2$–LiH mixture at 150–200 °C with hydrogen release. Although many experiments and calculations have been carried out [60–66], the crystal structure of Li_2NH is still ambiguous since it is difficult to identify the position of hydrogen and lithium atoms and the N–H bond orientations. Juza et al. [60] proposed that Li_2NH had an anti-fluorite structure (space group $Fm\bar{3}m$) with a lattice constant of $a = 5.047$ Å determined by XRD. Li atoms occupy the 8c sites, nitrogen atoms occupy the 4a sites, but the position of hydrogen atoms was not identified. Synchrotron XRD examinations show that the hydro-

gen atoms occupy randomly the 48 h sites around nitrogen atoms [61]. However, refinement of the neutron diffraction data indicates that Li_2NH is a cubic structure (space group $F\bar{4}3m$) with a lattice constant of $a = 5.0769$ Å, where the hydrogen atoms partially occupy the 16e sites [62]. Balogh et al. found that Li_2ND experienced an order–disorder transformation at around 85 °C [63], and the low-temperature crystal structure can be described as a disordered cubic structure (space group $Fd\bar{3}m$) with Li partially occupying the 32e sites or as a fully occupied orthorhombic (space group IM $a2$ or $Imm2$) structure, while the high-temperature crystal structure is a disorder cubic structure (space group $Fm\bar{3}m$) with D atoms randomized over the 192l sites. Investigations on the electronic structure reveal that Li_2NH is an ionic compound, in which the interaction between N and H atoms is covalent [61,63–66]. FTIR examinations on the characteristic absorptions of the N–H bonds in Li_2NH give different results. Chen et al. [67] observed a broad IR absorption centered at ~3160 cm^{-1} for Li_2NH produced by dehydriding the $LiNH_2$–LiH mixture at 320 °C. Isobe et al. [68] found that the IR absorption band of Li_2NH obtained by heating the ball-milled mixtures of LiH–$LiND_2$ and LiD–$LiNH_2$ to 450 °C located at ~3150 cm^{-1}. However, Kojima et al. [69] reported that Li_2NH prepared by decomposing $LiNH_2$ at 400 °C exhibited two broad IR characteristic bands at 3180 and 3250 cm^{-1}. The variable IR absorption bands are mainly attributed to the different preparation conditions. Generally, the crystal structures are different for the polymorph Li_2NH prepared under various conditions. Magnesium imide (MgNH) is synthesized by self-decomposition of $Mg(NH_2)_2$ or ball milling the $Mg(NH_2)_2$–MgH_2 mixture [59,70]. MgNH possesses a hexagonal structure with lattice constants of $a = 11.5800$ Å and $c = 3.6770$ Å, and gives rise to four signature IR absorptions at 3251, 3240, 3197 and 1560 cm^{-1} [55]. However, the atomic positions in crystal lattice have not been determined [71].

A novel ternary imide, $Li_2MgN_2H_2$ was developed after dehydriding the mixture of $Mg(NH_2)_2$–2LiH. Several different crystal structures have been reported for the newly produced $Li_2MgN_2H_2$. Using synchrotron XRD associated with neutron diffraction, Rijssenbeek et al. [72] observed that $Li_2MgN_2H_2$ underwent a structural transition from an orthorhombic structure to a primitive cubic structure followed by a face centered cubic structure with increasing temperatures. Liu et al. [73] obtained successfully a orthorhombic and cubic hybrid structure in $Li_2MgN_2H_2$ by sintering the mixture of $Mg(NH_2)_2$–2$LiNH_2$ milled for 36 h at a temperature range of 150–315 °C. The reaction taking place during the process is described as the following.

$$Mg(NH_2)_2 + 2LiNH_2 \overset{150^\circ C \text{ to } 315^\circ C}{\longrightarrow} Li_2MgN_2H_2 + 2NH_3 \quad (3)$$

Different synthesis methods were developed for $Li_2MgN_2H_2$ in recent years. Ma et al. [74] got the single phase $Li_2MgN_2H_2$ by heating the 3$Mg(NH_2)_2$–2Li_3N mixture to 240 °C under dynamic vacuum according to the following reaction.

$$3Mg(NH_2)_2 + 2Li_3N \rightarrow 3Li_2MgN_2H_2 + 2NH_3 \quad (4)$$

The polymorph structures of $Li_2MgN_2H_2$ are plotted in Fig. 3 [72]. As shown in Fig. 3(A), it is seen that the orthorhombic $Li_2MgN_2H_2$ is crystallized in a space group $Iba2$ with lattice constants of $a = 9.787$ Å, $b = 4.993$ Å and $c = 5.202$ Å, in which N and H atoms occupy the 8c sites, and Li and Mg atoms occupy the 4b and 8c sites in a mixed manner. The orthorhombic $Li_2MgN_2H_2$ can be described as a supercell of the high-temperature cubic structure of Li_2NH [61,62,72]. The doubling a-axis results from the ordering of the cation vacancies induced by the substitution of one Mg atom for two Li atoms [72]. The characteristic IR absorption bands of the orthorhombic $Li_2MgN_2H_2$ appear at around 3180 and 3163 cm^{-1} [75,76]. The cubic $Li_2MgN_2H_2$ crystallized in space group $P\bar{4}_3m$ has

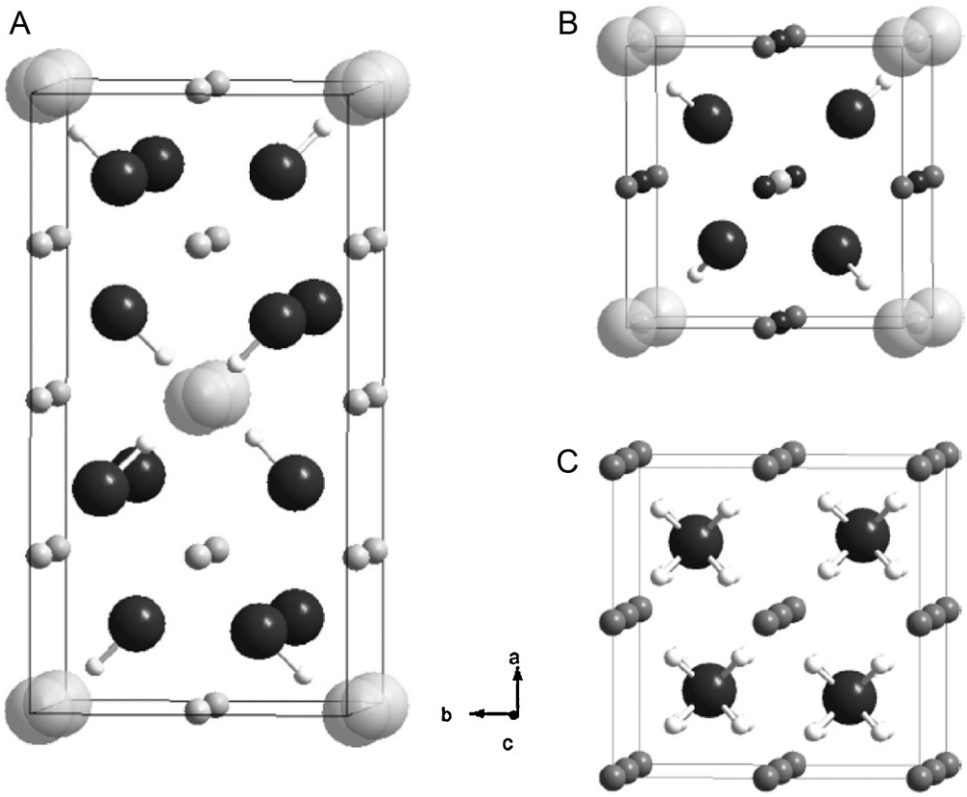

Fig. 3. Crystal structures of orthorhombic $Li_2MgN_2H_2$ in space group $Iba2$(A), cubic $Li_2MgN_2H_2$ in space group $P\bar{4}_3m$ (B) and $Fm\bar{3}m$ (C) [72]. Nitrogen atoms (dark grey), hydrogen atoms (white), mixed lithium and magnesium sites (small light grey) and vacancies (large transparent grey) are shown. Note that the imide protons are associated with the cation vacancies.

a primitive cubic unit cell with $a = 5.027$ Å (Fig. 3(B)), but the cubic $Li_2MgN_2H_2$ crystallized in space group $Fm\bar{3}m$ (Fig. 3(C)) exhibits a face-centered cubic cell with a lattice constant of $a \approx 5$ Å. The Li atoms, Mg atoms and vacancies are randomly distributed over the tetrahedral sites in the ratio of 2:1:1 [72]. Xiong et al. reported a different cubic structure of $Li_2MgN_2H_2$ with a lattice parameter of $a = 10.05$ Å, whereas the detailed information of the atomic positions has not been provided [77]. A broad IR absorption centered at 3174 cm^{-1} was detected for the cubic $Li_2MgN_2H_2$ [78]. Moreover, first-principles calculations have been performed on the crystal and electronic structures of $Li_2MgN_2H_2$ [79–81]. It is found that the orthorhombic structure is the ground-state configuration [79]. Several low-energy ordered structures were identified for orthorhombic $Li_2MgN_2H_2$, which are in agreement with the disordered structure obtained from the X-ray diffraction experiment [80]. Electronic structure calculations of $Li_2MgN_2H_2$ show that the bonding of N–H is strongly covalent and the Li–N and Mg–N are primarily ionic [81].

The ternary imide of $Li_2Mg_2N_3H_3$ was produced after heating the $Mg(NH_2)_2$–LiH mixture to 330 °C [77]. XRD examinations revealed that it possesses a tetragonal structure with lattice constants of $a = 5.15$ Å and $c = 9.67$ Å [77,78,82]. Two broad absorptions centered at 3195 and 3164 cm^{-1} were detected for the newly developed $Li_2Mg_2N_3H_3$ in the FTIR spectrum [78].

2.3. Nitrides

Lithium nitride (Li_3N) was prepared by reacting Li metal with N_2 gas at a temperature range of 100–200 °C or dehydrogenation of the $LiNH_2$–2LiH mixture above 420 °C [28,83]. There are two different crystal structures for Li_3N. One is a hexagonal structure crystallized in space group $P6/mmc$ with lattice constants of $a = 3.552$ Å and $c = 6.311$ Å [84]. Li atoms occupy the 2b and 4f sites, N atoms occupy the 2c sites. The other is also hexagonal Li_3N but crystallized in the space group of $P6/mmm$ with lattice constants of $a = 3.641$ Å and $c = 3.872$ Å, in which N atoms occupy the 1a sites and Li atoms occupy the 1b and 2c sites [85]. Magnesium nitride (Mg_3N_2) with a cubic crystal structure can be produced by the reaction between Mg metal and N_2 gas at a temperature range of 550–620 °C, full dehydrogenation of the $Mg(NH_2)_2$–$2MgH_2$ mixture, or the self-decomposition of $Mg(NH_2)_2$ at about 600 °C [53,83,86,87]. The cubic Mg_3N_2 crystallized in space group $Ia\bar{3}$ with a lattice constant of $a = 9.968$ Å, in which Mg atoms occupy the 48e sites and N atoms occupy the 8b and 24d sites [87]. The LiMgN ternary nitride with an orthorhombic structure was synthesized by heat treatment the Li_3N–Mg_3N_2 mixture at 627 °C under 1.2 bar N_2 atmosphere for 20 h [83]. The orthorhombic LiMgN is crystallized in space group $Pnma$ with lattice constants of $a = 7.158$ Å, $b = 3.507$ Å, and $c = 5.014$ Å, in which all of the Li, Mg, and N atoms occupy the 4c sites [83]. The Mg atom is coordinated with four N atoms and the Li atoms are situated in largely distorted nitrogen tetrahedron. Juza et al. [88] reported another cation-disordered cubic phase LiMgN, which was crystallized in space group $Fm\bar{3}m$ with a lattice constant of $a = 4.970$ Å. The N atoms occupy the 4a sites and the mixed Li and Mg atoms occupy the 8c sites.

3. De-/hydrogenation behaviors determined by the material compositions

It is well known that the composition change is an effective approach for tuning the thermodynamics of hydrogen storage materials, which has been extensively applied in the conventional metal hydrides and borohydrides [23,89]. Excitingly enough, replacing $LiNH_2$ in the $LiNH_2$–2LiH combination system with $Mg(NH_2)_2$ results in a significant decrease in the desorption enthalpy change, which decreases consequently the operating temperatures of the de-/hydrogenation reactions [90]. Moreover, it was found that a mixture of $2LiNH_2$–MgH_2 was equivalent to $Mg(NH_2)_2$–2LiH combination because of the metathesis reaction between $LiNH_2$ and MgH_2 [91]. Various dehydrogenated products and increased hydrogen storage capacity were achieved by increasing the stoichiometries of $Mg(NH_2)_2$–LiH or $LiNH_2$–MgH_2. Thus, the hydrogenation/dehydrogenation behaviors of the amide–hydride combinations depend strongly on the chemical compositions.

3.1. $Mg(NH_2)_2$–LiH combination systems

Xiong et al. [29] and Luo et al. [30,91] demonstrated that ca. 5.5 wt% of hydrogen could be stored reversibly in the $Mg(NH_2)_2$–2LiH and $2LiNH_2$–MgH_2 mixture through the following reaction.

$$2LiNH_2 + MgH_2 \rightarrow Mg(NH_2)_2 + 2LiH \leftrightarrow Li_2MgN_2H_2 + 2H_2 \quad (5)$$

For the $2LiNH_2$–MgH_2 combination, the rehydrogenated product is the $Mg(NH_2)_2$–2LiH mixture rather than the initial reactants of $2LiNH_2$–MgH_2 because the $Mg(NH_2)_2$–2LiH combination is thermodynamically more favored than $2LiNH_2$–MgH_2 [92]. Further thermodynamic investigations indicated that the desorption enthalpy change for the second step of reaction (5) is decreased to 44 kJ/mol-H_2, which offers the operation temperature of 90 °C at an equilibrium hydrogen pressure of 1 bar. This operating temperature satisfies the practical requirements of PEMFC [13]. The ex-situ XRD measurements demonstrated that the following two-step reaction occurred in the hydrogenation/dehydrogenation process [78].

$$2Li_2MgN_2H_2 + H_2 \leftrightarrow LiNH_2 + LiH + Li_2Mg_2(NH)_3 \quad (6)$$

$$LiNH_2 + Li_2Mg_2(NH)_3 + 3H_2 \leftrightarrow 3LiH + 2Mg(NH_2)_2 \quad (7)$$

For optimizing the hydrogen storage properties of the Li–Mg–N–H system, investigations on different stoichiometries of $Mg(NH_2)_2$–LiH were conducted by several groups. Xiong et al. [77] studied the hydrogen absorption/desorption properties of the $Mg(NH_2)_2$–nLiH ($n = 1, 2, 3$) mixtures, and found that higher content of LiH facilitated the reduction in the ammonia emission. ~3.0 wt% of hydrogen was liberated from the 1:1 $Mg(NH_2)_2$–LiH mixture along with a lot of ammonia release as expressed by the following reaction.

$$Mg(NH_2)_2 + LiH \rightarrow \frac{1}{2}Li_2Mg_2N_3H_3 + H_2 + \frac{1}{2}NH_3 \quad (8)$$

Unfortunately, only ~0.5 wt% of hydrogen was recharged into the dehydrogenated product under 80 bar of hydrogen [77]. While hydrogenation was carried out under 350 bar of hydrogen, the hydrogen absorption amount of $Li_2Mg_2N_3H_3$ was increased to ~3.4 wt% [93].

$$Li_2Mg_2N_3H_3 + 2H_2 \leftrightarrow Mg(NH_2)_2 + 2LiH + MgNH \quad (9)$$

It is worth noting that the rehydrogenated product is the mixture of $1/2Mg(NH_2)_2$–LiH–1/2MgNH rather than the starting reactants of $Mg(NH_2)_2$–LiH (molar ratio 1:1) owing to more favorable thermodynamic conditions. Leng et al. [54] designed a novel Li–Mg–N–H combination composed of $Mg(NH_2)_2$ and LiH with a molar ratio of 3:8, which can reversibly store ~6.9 wt% of hydrogen according to the following reaction:

$$3Mg(NH_2)_2 + 8LiH \leftrightarrow 4Li_2NH + Mg_3N_2 + 8H_2 \quad (10)$$

More interesting, the hydrogen storage capacity is increased to ~9.1 wt% as the molar ratio of $Mg(NH_2)_2$/LiH is increased to 1:4 [94].

$$3Mg(NH_2)_2 + 12LiH \leftrightarrow 4Li_3N + Mg_3N_2 + 12H_2 \quad (11)$$

However, first-principles calculations proposed a different dehydrogenation pathway for the $Mg(NH_2)_2$–4LiH mixture [95].

$$\begin{aligned} &Mg(NH_2)_2 + 4LiH \rightarrow Li_2MgN_2H_2 + 2LiH + H_2 \\ &\rightarrow Li_2NH + LiMgN + LiH + 2H_2 \\ &\rightarrow LiMgN + Li_3N + 3H_2 \end{aligned} \quad (12)$$

Apparently, changing the initial molar ratio of $Mg(NH_2)_2$ to LiH results in the different dehydrogenation reaction routes and different resultant products after complete dehydrogenation. Here, it has to be mentioned that the higher hydrogen capacity can only be achieved by applying higher temperature for the 3:8 and 1:4 molar ratios [54,94,96]. For the molar ratio 3:8, 6.9 wt% of hydrogen was released in the heating process up to 450 °C [96]. It is even as high as 500 °C for the complete hydrogen desorption from the sample with 1:4 molar ratio [94,96–98]. The dehydrogenation amounts at 250 °C for the molar ratios of 1:2, 3:8 and 1:4 were 5.4, 5.1, and 4.5 wt%, respectively [96], exhibiting a distinct reduction in the available hydrogen capacity at the relatively low operating temperature. The fact that a same plateau pressure was observed for the samples with various molar ratios indicates their similar thermodynamic nature [96–98]. The recent study on the $Mg(NH_2)_2$–xLiH mixtures (x = 1.5, 1.8, 2.0, 2.2, 2.5, and 2.7) reveals that the optimal composition is 1:2 of $Mg(NH_2)_2$ to LiH concerning hydrogen capacity, operating temperature and ammonia generation [99]. Deviation from this composition results either in severe ammonia emission or deterioration of hydrogen storage efficiency. The ternary imide $Li_2Mg(NH)_2$ was found in both dynamic and quasi-equilibrium dehydrogenation of this hydrogen storage system, which is responsible for the good cycle stability of this system. As a result, it is impossible to improve the hydrogen sorption properties simply by adjusting the stoichiometry of the starting materials in the $Mg(NH_2)_2$–LiH system as reported by Hu et al. [99].

3.2. $LiNH_2$–MgH_2 combination systems

Since there is an equimolar $H^{\delta+}$ and $H^{\delta-}$ in $LiNH_2$ and MgH_2, the enhanced hydrogen storage capacity is expected by mixing the 1:1 molar ratio of $LiNH_2$–MgH_2. Alapati et al. predicted that ~8.19 wt% of hydrogen could be released from the novel $LiNH_2$–MgH_2 combination by the first-principles calculation [100].

$$LiNH_2 + MgH_2 \rightarrow LiMgN + 2H_2 \quad (13)$$

The desorption enthalpy change was estimated to be 29.7 kJ/mol-H_2, which is the moderate thermodynamics for reversible hydrogen storage systems. Further calculations proposed a stepwise dehydrogenation reaction for the $LiNH_2$–MgH_2 combination [95]:

$$\begin{aligned} LiNH_2 + MgH_2 &\rightarrow \frac{1}{2}Mg(NH)_2 + \frac{1}{2}MgH_2 + LiH \\ &\rightarrow \frac{1}{4}Mg(NH)_2 + \frac{1}{4}Mg_3N_2 + LiH + H_2 \\ &\rightarrow \frac{1}{4}Li_2Mg(NH)_2 + \frac{1}{4}Mg_3N_2 + \frac{1}{2}LiH + \frac{3}{2}H_2 \\ &\rightarrow LiMgN + 2H_2 \end{aligned} \quad (14)$$

However, the experimental investigations showed some different results. Lu et al. [101,102] reported that ~8.2 wt% of hydrogen was released from the $LiNH_2$–MgH_2 mixture at 160–220 °C after a low energy milling (rolling jar), and the resultant product is LiMgN as expressed by reaction (13). Osborn et al. [103] observed a new dehydrogenation product, $Li_2Mg_2N_3H_3$ for the 3 h milled $LiNH_2$–MgH_2 mixture. The reaction is as the following:

$$LiNH_2 + MgH_2 \xrightarrow{\text{heated to and kept at 210°C}} \frac{1}{3}Li_2Mg_2N_3H_3 + \frac{1}{3}MgH_2 + \frac{1}{3}LiH + H_2 \quad (15)$$

Liu et al. [104,105] found that the reaction routes for the hydrogenation/dehydrogenation of the $LiNH_2$–MgH_2 mixture depend strongly on the mechanochemical treatment process, and identified various dehydrogenation reactions for the $LiNH_2$–MgH_2 mixture milled for different durations. It is found that after 2 h of ball milling, the $LiNH_2$–MgH_2 mixture remains unchanged, *i.e.*, no new specie is developed, and hydrogen is gradually desorbed according to the reaction (15) as heated and kept at 210 °C. Milled for 12 h, the $LiNH_2$–MgH_2 mixture converts to the 1/2$Mg(NH_2)_2$–LiH–1/2MgH_2 mixture without hydrogen evolution as predicted by Akbarzadeh et al. [95]. However, in the subsequent heating process, hydrogen desorption proceeds according the following reaction instead of reaction (14).

$$\begin{aligned} LiNH_2 + MgH_2 &\xrightarrow{\text{milled for 12 h}} \frac{1}{2}Mg(NH_2)_2 + LiH + \frac{1}{2}MgH_2 \\ &\xrightarrow{\text{heated to 250°C}} \frac{1}{2}Li_2MgN_2H_2 + \frac{1}{2}MgH_2 + H_2 \\ &\xrightarrow{\text{heated to 400°C}} \frac{1}{3}Mg_3N_2 + \frac{1}{3}Li_2NH + \frac{1}{3}LiH + \frac{5}{3}H_2 \end{aligned} \quad (16)$$

Further prolonging the ball milling time induces the reaction of $Mg(NH_2)_2$ with MgH_2 to release hydrogen since the reaction between $Mg(NH_2)_2$ and MgH_2 is thermodynamically favorable but unfavorable from the kinetic point of view. Hydrogen desorption from the post-36 and 48 h milled mixtures could be described as follows [105]:

BM 36 h:

$$\begin{aligned} LiNH_2 + MgH_2 &\xrightarrow{\text{milled for 12h}} \frac{1}{2}Mg(NH_2)_2 + LiH + \frac{1}{2}MgH_2 \\ &\xrightarrow{\text{milled for 36h}} \frac{1}{2}MgNH + \frac{1}{4}Mg(NH_2)_2 + LiH + \frac{1}{4}MgH_2 + \frac{1}{2}H_2 \\ &\xrightarrow{\text{heated to 220°C}} \frac{1}{4}Li_2MgN_2H_2 + \frac{1}{2}MgNH + \frac{1}{2}LiH + \frac{1}{4}MgH_2 + H_2 \\ &\xrightarrow{\text{heated to 390°C}} \frac{1}{4}Mg_3N_2 + \frac{1}{4}Li_2MgN_2H_2 + \frac{1}{2}LiH + \frac{3}{2}H_2 \end{aligned} \quad (17)$$

BM 48 h:

$$\begin{aligned} LiNH_2 + MgH_2 &\xrightarrow{\text{milled for 12h}} \frac{1}{2}Mg(NH_2)_2 + LiH + \frac{1}{2}MgH_2 \\ &\xrightarrow{\text{milled for 48h}} \frac{3}{4}MgNH + \frac{1}{8}Mg(NH_2)_2 + LiH + \frac{1}{8}MgH_2 + \frac{3}{4}H_2 \\ &\xrightarrow{\text{heated to 225°C}} \frac{1}{8}Li_2MgN_2H_2 + \frac{3}{4}MgNH + \frac{3}{4}LiH + \frac{1}{8}MgH_2 + H_2 \\ &\xrightarrow{\text{heated to 400°C}} \frac{7}{24}Mg_3N_2 + \frac{1}{8}Li_2MgN_2H_2 + \frac{1}{6}Li_2NH + \frac{5}{12}LiH + \frac{19}{12}H_2 \end{aligned} \quad (18)$$

Obviously, the dehydrogenation performance of the $LiNH_2$–MgH_2 combination is closely related to the ball milling treatment because there are two competing reactions during the ball milling and subsequent heating process. Unfortunately however, only partial hydrogen could be re-absorbed after dehydrogenation under 105 atm of hydrogen, which means that hydrogen recharge after dehydrogenation to this system can not be completed.

4. Tuning on thermodynamics and kinetics of hydrogen storage process

Although the operating temperature thermodynamically predicated for the $Mg(NH_2)_2$–2LiH system is only about 90 °C at 1 bar of the equilibrium hydrogen pressure, acceptable hydrogen desorption rate can be realized at 200 °C and above because of the

rather high kinetic barrier. Numerous efforts have been devoted to reducing the operating temperatures for hydrogen desorption from the $Mg(NH_2)_2$–2LiH material by tuning the thermodynamics and kinetics.

It is well known that catalyst doping is an effective approach to improve the hydrogenation/dehydrogenation thermodynamics and kinetics. Sudik et al. [106] observed a 40 °C reduction in the peak dehydrogenation temperature of the $Mg(NH_2)_2$–2LiH combination by seeding the dehydrogenated product, *viz.*, $Li_2MgN_2H_2$, Nevertheless, after one hydrogenation/dehydrogenation cycle the peak hydrogen desorption temperature was shifted 10 °C toward higher temperature due to the diminishment of $Li_2MgN_2H_2$ caused by agglomeration and consumption (converting to $Mg(NH_2)_2$ and LiH after hydrogenation). Chen et al. [107] introduced different carbon materials such as single-walled carbon nanotubes (SWNTs), multi-walled carbon tubes (MWNTs), graphite and activated carbon into the $Mg(NH_2)_2$–2LiH mixture as additives, and found that about 90% of the hydrogen capacity can be released at 200 °C in 20 min from the sample with addition of SWNTs while less than 60% of the hydrogen capacity was released from the pristine sample. In addition, many chemicals, such as NaH, $NaNH_2$, TiN, TiF_3, TaN, Li_3N, V, V_2O_5, VCl_3, $Ti_3Cr_3V_4$ hydride and graphite-supported Ru nanoparticles were also added as catalysts for improving the kinetics of the $Mg(NH_2)_2$–2LiH system [108–114]. But the operating temperatures for hydrogen absorption/desorption are still far from the practical requirement. Recently, Hu et al. reported that the addition of a small amount of $LiBH_4$ considerably improved the hydrogen absorption/desorption performances of the $Mg(NH_2)_2$–2LiH mixture, *i.e.*, with a 3-fold increase in the de-/hydrogenation rates [115]. Thermodynamic and kinetic analyses showed that the decrease in both activation energies and reaction enthalpies were responsible for the improvement of hydrogen storage properties [115,116]. Similar improvement on the hydrogen storage properties was obtained by adding a small amount of $NaBH_4$ with a different catalytic mechanism [117]. It was revealed that $LiBH_4$ reacted with the $LiNH_2$ product to form $Li_4(BH_4)(NH_2)_3$, which weakens the N–H bonds [115]. Unlike $LiBH_4$, $NaBH_4$ remains almost unchanged in the whole dehydrogenation/hydrogenation process of the $NaBH_4$–added $Mg(NH_2)_2$–2LiH combination [117]. DFT calculations show that the appearance of $NaBH_4$ in the $Mg(NH_2)_2$–2LiH system facilitates the formation of Mg vacancies, which not only weakens the N–H bonds but also promotes the diffusion of atoms and/or ions, and consequently improving the dehydrogenation kinetics of the $NaBH_4$–doped $Mg(NH_2)_2$–2LiH system. Recently, Zhang et al. demonstrated that the hydrogen absorption/desorption rates of the $Mg(NH_2)_2$–2LiH mixture could be further improved by the co-catalytic function of $LiBH_4$ and ZrCo hydride [118]. It is believed that the nanosized ZrCo hydride particle not only acts as the active sites for nucleation and growth of the dehydrogenation products but also weakens the N–H bonds due to the interaction between the lone electron pair of the $-NH_2$ group and the heterocyclic orbits of Zr and Co. Significantly, a dramatic improvement in the hydrogenation/dehydrogenation performances of the $Mg(NH_2)_2$–2LiH combination was achieved by adding NaOH or KH. The onset temperature for hydrogen desorption of the $Mg(NH_2)_2$–2LiH–0.5NaOH mixture was lowered by 36 °C, less than 100 °C [119]. Excitingly enough, the peak temperature for the hydrogen desorption of the $Mg(NH_2)_2$–2LiH–0.1KH system is only 132 °C as shown in Fig. 4, exhibiting the lowest dehydrogenation temperature in the Li–Mg–N–H combination systems so far [120]. However, the role played by KH in the Li–Mg–N–H system still needs to be understood in detail.

The dehydrogenation/hydrogenation kinetics of the Li–Mg–N–H systems was also enhanced by reducing the particle size and increasing the mixing degree of materials. Liu et al. [73] revealed that the $Li_2MgN_2H_2$ sample milled for 36 h started to absorb hydrogen at only 80 °C while the onset temperature for hydrogen absorption of the hand-milling sample was about 150 °C (Fig. 5). The decrease in the activation energy caused by the shortening of the diffusion distance and the enlarging of the specific surface area is believed to be the primary reason. Similar conclusions were drawn by Xie et al. [121]. However, the particle size is gradually augmented in the cycling process for de-/hydrogenation due to the aggregation. Wang et al. [122] found that the addition of triphenyl phosphate could effectively prevent the aggregation of dehydrogenated products and the crystallization of $Mg(NH_2)_2$ in the hydrogenation/dehydrogenation process, which results in a kinetic improvement in hydrogen absorption/desorption of the $Mg(NH_2)_2$–2LiH system.

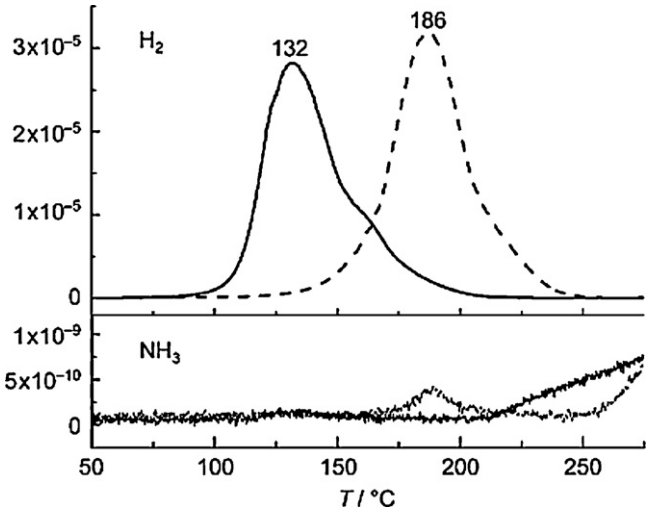

Fig. 4. Temperature dependences of H_2 and NH_3 release from the $Mg(NH_2)_2$–2LiH mixture and that with KH modified [120].

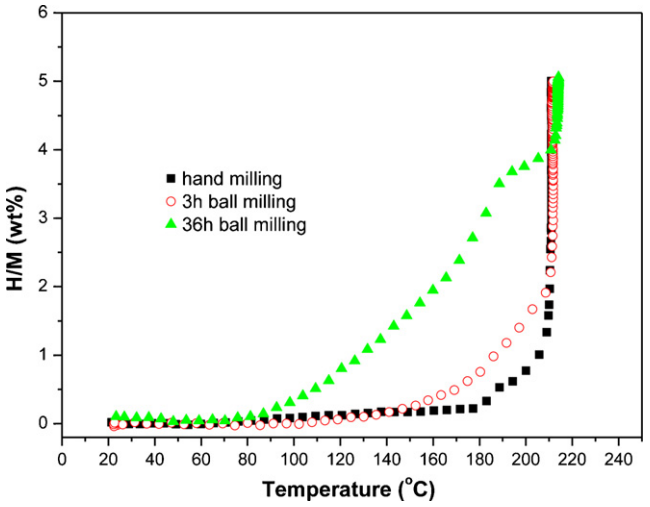

Fig. 5. Hydrogenation curves of $Li_2MgN_2H_2$ samples with different milling treatments [73].

5. Hydrogen storage mechanisms of the $Mg(NH_2)_2$–2LiH combination

Since Chen et al. introduced nitrogen into the hydrogen storage system in 2002, considerable efforts have been devoted to understanding the hydrogen storage mechanisms of the newly developed amide–hydride combination systems. There are two controversial reaction mechanisms for interpreting the

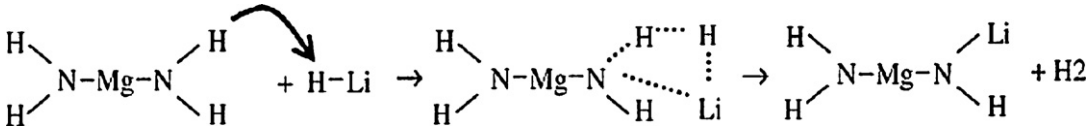

Fig. 6. Reaction mechanism of the $Mg(NH_2)_2$–2LiH combination system [90].

hydrogen absorption/desorption process. One is the coordinated two-molecular or multi-molecular reaction mechanism [29,67,91,123–126], and the other is the ammonia-mediated reaction mechanism [45,54,127–130].

5.1. Coordinated solid state reaction mechanism

Chen et al. proposed that the dehydrogenation process of the amide–hydride combinations proceeded via a direct solid–solid reaction driven by the strong affinity between $H^{\delta+}$ in amide and $H^{\delta-}$ in hydride [29].

$$H^+ + H^- \rightarrow H_2(\Delta H = -17.37\,\text{ev}) \quad (19)$$

The fact that the hydrogen desorption temperatures of the amide–hydride mixtures are pronouncedly lower than the thermal decomposition temperatures of the corresponding amides is a reasonable evidence. Moreover, the isotopic exchange between $H^{\delta+}$ in amides and $D^{\delta-}$ in deuterides in the dehydrogenation process of the amide–deutride mixture further supports the coordinated reaction mechanism [67,123–125]. Fig. 6 presents schematically the reaction process for the $Mg(NH_2)_2$–2LiH mixture on the basis of the strong affinity of $H^{\delta+}$ and $H^{\delta-}$ as proposed by Xiong et al. [90]. Luo et al. [91] suggested a new ternary imide of $Li_2MgN_2H_{3.2}$ for the hydrogen desorption of the $Mg(NH_2)_2$–2LiH mixture as follows.

$$Mg(NH_2)_2 + 2LiH \leftrightarrow Li_2MgN_2H_{32} + 1.4H_2 \quad (20)$$

$$Li_2MgN_2H_{3.2} \leftrightarrow Li_2MgN_2H_2 + 0.6H_2 \quad (21)$$

However, Hu et al. [78] detected the formation and consumption of $Li_2Mg_2N_3H_3$ and $LiNH_2$ in the hydrogen absorption/desorption process by characterizing the structures of the dehydrogenated products at different stages as described by reactions (6) and (7). It can be therefore believed that the hydrogen storage in the $Mg(NH_2)_2$–2LiH combination system is a stepwise process.

Moreover, David et al. [125] and Wu et al. [126] suggested a more detailed ion migration model by refining the synchrotron XRD data of the amide–hydride combination systems, in which the creation of a Frenkel defect pair is the key to the movement of a metallic cation to an adjacent, vacant, tetrahedral or octahedral site. Taking the Li–N–H system as an example, such a process create two adjacent, unstable, charged species, $[LiLiNH_2]^+$ and $[\square NH_2]^-$, where $\square$ is a formerly Li^+-occupied tetrahedral site. Charge balance at the atomic level may be restored by the expulsion of a proton from $[LiLiNH_2]^+$, which can react with H^- in LiH to generate H_2. As for the Li–Mg–N–H system, in hydrogenation process, $Li_2Mg(NH)_2$ forms a vacancy-containing structure derivative due to the similar size of Mg^{2+} and Li^+ and can be written as $(LiMg_{0.5}\square_{0.5})NH$. In such a structure, Li^+ ions migrate through the cation vacancies and interact with H_2 applied to form LiH and H^+. The proton produced will be attracted toward the negatively charged region to produce $Mg(NH_2)_2$. The hydrogenation process can be expressed by the following reactions [126].

$$(LiMg_{0.5}\square_{0.5})NH \rightarrow [(\square_{Li}Mg_{0.5}\square_{0.5})NH]^- + Li^+ \quad (22)$$

$$Li^+ + H_2 \rightarrow LiH + H^+ \quad (23)$$

$$H^+ + [(\square_{Li}Mg_{0.5}\square_{0.5})NH]^- \rightarrow [(Mg_{0.5}\square_{0.5})NH_2] \quad (24)$$

It is clear that the migration of small ions both in amides and hydrides plays an important role for hydrogenation/dehydrogenation of the amide–hydride combination systems.

5.2. Ammonia-mediated reaction mechanism

Alternatively, Leng et al. [127] proposed the ammonia-mediated reaction mechanism, in which $Mg(NH_2)_2$ decomposes to ammonia and imide/nitride, and then the ammonia formed reacts with hydride to produce hydrogen. Taking the $3Mg(NH_2)_2$–8LiH system as an example, the hydrogenation process can express as follows [127].

$$\begin{aligned}
&Mg_3N_2 + 4Li_2NH + 8H_2 \rightarrow 4LiH + 4LiNH_2 + Mg_3N_2 + 4H_2\\
&\rightarrow 4LiH + (2Li_2NH + 2H_2) + (2NH_3 + \frac{1}{2}Mg_3N_2) + \frac{1}{2}Mg_3N_2 + 2H_2\\
&\rightarrow 4LiH + 2LiH + \frac{3}{2}Mg(NH_2)_2 + 2LiNH_2 + \frac{1}{2}Mg_3N_2 + 2H_2\\
&\cdots\\
&\rightarrow 4\left(\sum_{k=0}^{n}\frac{1}{2^k}\right)LiH + 3\left(\sum_{k=1}^{n}\frac{1}{2^k}\right)Mg(NH_2)_2\\
&+\frac{1}{2^{n-2}}LiNH_2 + \frac{1}{2^n}Mg_3N_2 + \frac{1}{2^{n-2}}H_2\\
&\rightarrow 3Mg(NH_2)_2 + 8LiH
\end{aligned} \quad (25)$$

In the hydrogenation process of the Mg_3N_2–$4Li_2NH$ sample at 200 °C under 10 bar H_2, the growing up of the $LiNH_2$ and LiH phases were observed in the in situ XRD profiles before the formation of the $3Mg(NH_2)_2$ and 8LiH phases as the final hydrogenation state [129]. The growth of the $LiNH_2$ and LiH phases in hydrogenation process is believed to be the evidence for the ammonia-mediated reaction mechanism. Isobe et al. [130] elucidated that the dehydrogenated products of the $Mg(NH_2)_2$–nLiH systems depend strongly on the content of LiH, the operating temperature and the H_2 pressure. If enough LiH reacts with Mg-amide under an equilibrium condition, the dehydrogenation reaction process can be described as [130]:

$$\begin{aligned}
&\text{Mg-amide} \rightarrow \text{Li-amideandMg-imide} \rightarrow \text{Li-imideandMg-imide}\\
&\rightarrow \text{Li-imideandMg-nitride} \rightarrow \text{Li-nitrideandMg-nitride}.
\end{aligned}$$

5.3. Kinetic mechanisms of the $Mg(NH_2)_2$–2LiH combined system

From the point of view of solid–solid reaction, Chen et al. [123] proposed that the kinetic barrier for hydrogen desorption from the $Mg(NH_2)_2$–2LiH system might originate from the interface reaction in the preliminary stage and mass transport through the product layer. As a result, the particle size and the mixing degree of reacting species could affect the overall kinetics of a chemical reaction [73,122]. Liu et al. revealed further that hydrogen desorption from the $Mg(NH_2)_2$–2LiH mixture was a three-dimensional diffusion-controlled reaction [73]. The improved kinetics for hydrogenation/dehydrogenation was achieved by reducing the particle size of $Li_2MgN_2H_2$ or $Mg(NH_2)_2$ as the activation energies of hydrogen desorption from the $Mg(NH_2)_2$–2LiH combined system are obviously decreased from 132.6 kJ/mol for the hydrogenated hand-milling $Li_2MgN_2H_2$ sample to 51.6 kJ/mol for the hydrogenated post-36 h milled $Li_2MgN_2H_2$ sample.

5.4. Capacity degradation mechanisms

The cycling stability is one of the key issues for the practical applications of hydrogen storage media. Luo and co-workers [131] reported the capacity retention of the $Mg(NH_2)_2$–2LiH system is only 75% after 270 cycles at 200 °C. The ammonia emission is believed to be responsible for the capacity loss during hydrogenation/dehydrogenation cycling since it losses nitrogen. It was found that the concentration of NH_3 in the hydrogen desorbed from the $2LiNH_2$–MgH_2 mixture was increased from 180 ppm at 180 °C to 720 ppm at 240 °C [131]. Liu et al. revealed that the self-decomposition of $Mg(NH_2)_2$ under high hydrogen pressure was likely to be the primary source of NH_3 release in the cycling [132]. Fortunately, the ammonia released from the Li–Mg–N–H systems can be reduced by doping catalysts, decreasing operating temperatures, increasing the molar ratio of LiH and enhancing the mixing level as reported extensively [77,106,107,115,120,122,132].

6. Summaries and outlook

Metal–N–H-based hydrogen storage systems have been attracting considerable attentions since Chen et al. reported that Li_3N could reversibly store ~11.4 wt% of hydrogen. Of them, the Li–Mg–N–H combination was regarded as one of the most promising candidates for vehicular applications due to the relatively high hydrogen content, good reversibility and moderate operating temperatures. The dehydrogenation temperature predicted on the basis of thermodynamics is about 90 °C at 1 bar of equilibrium pressure. However, the acceptable dehydrogenation rate can be obtained above 200 °C due to the relatively high kinetic barrier. Tremendous efforts have been devoted to improving the hydrogen storage properties by adjusting composition, adding catalysts, reducing particle size and understanding reaction mechanisms, etc. It is found that the hydrogen storage capacity of the Li–Mg–N–H systems depends strongly on the stoichiometries of $Mg(NH_2)_2$–LiH. Hydrogen storage capacity is increased from 3.0 wt% to 9.1 wt% as the molar ratios of $Mg(NH_2)_2$–LiH was changed from 1:1 to 1:4, and various dehydrogenated products were obtained after dehydrogenation. Several models have been proposed for understanding the hydrogenation/dehydrogenation process. One is the coordinated two-molecule or multi-molecule reaction mechanism, in which the hydrogen desorption proceeds through a direct solid–solid reaction. The driving force is believed to be the strong affinity between the positively charged $H^{\delta+}$ in amides and the negatively charged $H^{\delta-}$ in hydrides. Alternatively, the ammonia-media reaction mechanism was suggested. It is believed that the amides first decomposed to ammonia and imide/nitride and then the ammonia newly liberated reacted with hydride to produce hydrogen. Moreover, a more detailed ion migration model is proposed by refining the synchrotron XRD data, in which the presence of Frenkel defect pairs in amide is the key in the dehydrogenation/hydrogenation process, and the hydrogenation/dehydrogenation reactions depend strongly on the migration of small ions in amides, imides and hydrides. The origin of kinetic barriers for dehydrogenation is attributed to the interface reaction between amide and hydride for forming a ternary imide in the preliminary stage and mass transport through the imide layer in the subsequent stage. The diffusion is identified to be the rate-determined step for hydrogen desorption. Therefore, weakening the N–H bonding and reducing the particle size are believed to be the effective approaches to improve the reaction thermodynamics and kinetics for hydrogen storage. Although the hydrogen storage performances have been dramatically improved by adding catalysts and reducing particle size, the hydrogen storage capacity and the hydrogenation/dehydrogenation kinetics of the $Mg(NH_2)_2$–2LiH combination system cannot satisfy the practical requirements for on-board hydrogen storage yet. As a consequence, the novel amide–hydride combination with high hydrogen content, moderate thermodynamics and fast kinetics is still expected. Specially, the underlying role played by dopants in the Li–Mg–N–H systems should also be understood in depth to guide the design and development of the high-performance catalysts used in the amide-hydride combination system. Moreover, the reaction mechanisms for hydrogen storage in the amide–hydride combinations need also to be further elucidated. We believed that first-principles calculation is likely a powerful tool for understanding the reaction mechanisms and predicting the advanced catalysts.

Acknowledgements

The authors would like to acknowledge financial support from the National Basic Research Program of China (Grant No.: 2010CB631304), from the National High Technology Research and Development Program of China (Grant No.: 2009AA05Z106), from the National Natural Foundation of China (Grant Nos.: 51025102 and 50871100), and from Zhejiang Innovation Program for Graduates (Grant No.: YK2009003).

References

[1] M.S. Dresselhaus, I.L. Thomas, Nature 414 (2001) 332–337.
[2] L. Schlapbach, A. Züttle, Nature 414 (2001) 353–358.
[3] C.J. Winter, Int J. Hydrogen Energy 34 (2009) S1–S52.
[4] L. Schlapbach, Nature 460 (2009) 809–811.
[5] I.P. Jain, Int. J. Hydrogen Energy 34 (2009) 7368–7378.
[6] U. Eberle, M. Felderhoff, F. Schüth, Angew. Chem. Int. Ed. 48 (2009) 6608–6630.
[7] F. Schüth, Eur. Phys. J. Special Topics 176 (2009) 155–166.
[8] M. Felderhoff, C. Weidenthaler, R. von Helmolt, U. Eberle, Phys. Chem. Chem. Phys. 9 (2007) 2643–2653.
[9] A. Züttle, Mater. Today 7 (2003) 24–33.
[10] http://www1.eere.energy.gov/hydrogenandfuelcells/pdfs/national_h2_roadmap.pdf.
[11] L.C. Pérez, L. Brandão, J.M. Sousa, A. Mendes, Renew. Sustain. Energy Rev. 15 (2011) 169–185.
[12] M. Millera, A. Bazylak, J. Power Sources 196 (2011) 601–613.
[13] https://www1.eere.energy.gov/hydrogenandfuelcells/storage/pdfs/targets_onboard_hydro_storage_explanation.pdf.
[14] K.L. Lim, H. Kazemian, Z. Yaakob, W.R.W. Daud, Chem. Eng. Technol. 33 (2010) 213–226.
[15] L. Schlaphach, Hydrogen in Intermetallic Compounds I, Topic in Applied Physics, Springer-Verlag, Berlin, 1988.
[16] L. Schlaphach, Hydrogen in Intermetallic Compounds II, Topic in Applied Physics, Springer-Verlag, Berlin, 1992.
[17] G. Sandrock, J. Alloys Compd. 293–295 (1999) 877–888.
[18] B. Bogdanović, M. Schwickardi, J. Alloys Compd. 253–254 (1997) 1–9.
[19] Y.F. Liu, Y.H. Cao, L. Huang, M.X. Gao, H.G. Pan, J. Alloys Compd. 509 (2011) 675–686.
[20] W.Y. Li, C.S. Li, H. Ma, J. Chen, J. Am. Chem. Soc. 129 (2007) 6710–6711.
[21] S.Y. Zheng, F. Fang, G.Y. Zhou, G.R. Chen, L.Z. Ouyang, M. Zhu, D.L. Sun, Chem. Mater. 20 (2008) 3954–3958.
[22] A. Züttel, P. Wenger, S. Rentsch, P. Sudan, Ph. Mauron, Ch. Emmenegger, J. Power Sources 118 (2003) 1–7.
[23] J.J. Vajo, S.L. Skeith, F. Mertens, J. Phys. Chem. B 109 (2005) 3719–3722.
[24] H.W. Li, K. Kikuchi, Y. Nakamori, N. Ohba, K. Miwa, S. Towata, S. Orimo, Acta Mater. 56 (2008) 1342–1347.
[25] Z.G. Zhang, S.F. Zhang, H. Wang, J.W. Liu, M. Zhu, J. Alloys Compd. 505 (2010) 717–721.
[26] Y.F. Liu, F.H. i Wang, Y.H. Cao, M.X. Gao, H.G. Pan, Q.D. Wang, Energy Environ. Sci. 3 (2010) 645–653.
[27] S. Orimo, Y. Nakamori, J.R. Eliseo, A. Züttel, C.M. Jensen, Chem. Rev. 107 (2007) 4111–4132.
[28] P. Chen, Z. Xiong, J. Luo, J. Lin, K.L. Tan, Nature 420 (2002) 302–304.
[29] Z. Xiong, G. Wu, J. Hu, P. Chen, Adv. Mater. 16 (2004) 1522–1525.
[30] W. Luo, J. Alloys Compd. 381 (2004) 284–287.
[31] F.E. Pinkerton, G.P. Meisner, M.S. Meyer, M.P. Balogh, M.D. Kundrat, J. Phys. Chem. B 109 (2005) 6–8.
[32] Z. Xiong, G. Wu, J. Hu, P. Chen, J. Power Sources 159 (2006) 167–170.
[33] G. Wu, Z. Xiong, T. Liu, Y. Liu, J. Hu, P. Chen, Y. Feng, A.T.S. Wee, Inorg. Chem. 46 (2007) 517–521.
[34] Y. Liu, J. Hu, G. Wu, Z. Xiong, P. Chen, J. Phys. Chem. C 111 (2007) 19161–19164.
[35] Y. Liu, J. Hu, Z. Xiong, G. Wu, P. Chen, K. Murata, K. Sakata, J. Alloys Compd. 432 (2007) 298–302.

[36] K. Tokoyoda, S. Hino, T. Ichikawa, K. Okamoto, H. Fujii, J. Alloys Compd. 439 (2007) 337–341.
[37] M. Fichtner, Adv. Eng. Mater. 7 (2005) 443–455.
[38] P. Chen, M. Zhu, Mater. Today 11 (2008) 36–43.
[39] A.W.C. van den Berg, C.O. Areán, Chem. Commun. (2008) 668–681.
[40] T.K. Mandal, D.H. Gregory, Annu. Rep. Prog. Chem. Sect. A 105 (2009) 21–54.
[41] J. Graetz, Chem. Soc. Rev. 38 (2009) 73–82.
[42] I.P. Jain, P. Jain, A. Jain, J. Alloys Compd. 503 (2010) 303–339.
[43] J. Yang, A. Sudik, C. Wolverton, D.J. Siegel, Chem. Soc. Rev. 39 (2010) 656–675.
[44] A.W. Titherley, J Chem. Soc. Trans. 65 (1894) 504–522.
[45] Y.H. Hu, E. Ruckenstein, J. Phys. Chem. A 107 (2003) 9737–9739.
[46] H.Y. Leng, T. Ichikawa, S. Hino, N. Hanada, S. Isobe, H. Fujii, J. Power Sources 156 (2006) 166–170.
[47] H. Toyoda, M. Watanabe, H. Sugai, J. Nucl. Mater. 241 (1997) 1031–1035.
[48] Y. Nakamori, T. Yamagishi, M. Yokoyama, S. Orimo, J. Alloys Compd. 377 (2004) L1–L3.
[49] J.B. Yang, X.D. Zhou, Q. Cai, W.J. James, W.B. Yelon, Appl. Phys. Lett. 88 (2006) 41914.
[50] T. Tsumuraya, T. Shishidou, T. Oguchi, J. Alloys Compd. 446–447 (2007) 323–327.
[51] J.P.O. Bohger, R.R. Eβmann, H. Jacobs, J. Mol. Struct. 348 (1995) 325–328.
[52] T. Markmaitree, W. Osborn, L.L. Shaw, J. Power Sources 180 (2008) 535–538.
[53] Y. Nakamori, G. Kitahara, S. Orimo, J. Power Sources 138 (2004) 309–312.
[54] H.Y. Leng, T. Ichikawa, S. Hino, N. Hanada, S. Isobe, H. Fujii, J. Phys. Chem. B 108 (2004) 8763–8765.
[55] G. Linde, R. Juza, Z. Anorg. Allg. Chem 409 (1974) 199–214.
[56] L. Xie, Y. Li, R. Yang, Y. Liu, X. Li, Appl. Phys. Lett. 92 (2008) 231910.
[57] M.H. Sørby, Y. Nakamura, H.W. Brinks, T. Ichikawa, S. Hino, H. Fujii, B.C. Hauback, J. Alloys Compd. 428 (2007) 297–301.
[58] T.A.T. Seip, R.A. Olsen, O.M. Løvvik, J. Phys. Chem. C 113 (2009) 21648–21656.
[59] H.Y. Leng, T. Ichikawa, S. Isobe, S. Hino, N. Hanada, H. Fujii, J. Alloys Compd. 404–406 (2005) 443–447.
[60] R. Juza, K. Opp, Z. Anorg. Allg. Chem. 266 (1951) 325–330.
[61] T. Noritake, H. Nozaki, M. Aoki, S. Towata, G. Kitahare, Y. Nakamori, S. Orimo, J. Alloys Compd. 393 (2005) 264–268.
[62] K. Ohyama, Y. Nakamori, S. Orimo, K. Yamsda, J. Phys. Soc. Jpn. 74 (2005) 483–487.
[63] M.P. Balogh, C.Y. Jones, J.F. Herbst, L.G. Hector, M. Kundrat Jr., J. Alloys Compd. 420 (2006) 326–336.
[64] J.F. Herbst, L.G. Hector Jr., Phys. Rev. B 72 (2005) 125120.
[65] B. Magyari-Köpe, V. Ozoliò, C. Wolverton, Phys. Rev. B 73 (2006) 220101.
[66] T. Muller, G. Ceder, Phys. Rev. B 74 (2006) 134104.
[67] P. Chen, Z. Xiong, J. Luo, J. Lin, K.L. Tan, J. Phys. Chem. B 107 (2003) 10967–10970.
[68] S. Isobe, T. Ichikawa, S. Hino, H. Fujii, J. Phys. Chem. B 109 (2005) 14855–14858.
[69] Y. Kojima, Y. Kawai, J. Alloys Compd. 395 (2005) 236–239.
[70] J. Hu, Z. Xiong, G. Wu, P. Chen, K. Murata, K. Sakata, J. Power Sources 159 (2006) 120–125.
[71] H. Jacobs, R. Juza, Z. Anorg. Allg. Chem. 370 (1969) 254–261.
[72] J. Rijssenbeek, Y. Gao, J. Hanson, Q. Huang, C. Jones, B. Toby, J. Alloys Compd. 454 (2008) 233–244.
[73] Y. Liu, K. Zhong, K. Luo, M. Gao, H. Pan, Q. Wang, J. Am. Chem. Soc. 131 (2009) 1862–1870.
[74] L. Ma, H. Dai, Z. Fang, X. Kang, Y. Liang, P. Wang, P. Wang, H. Cheng, J. Phys. Chem. C 113 (2009) 9944–9949.
[75] T. Markmaitree, W. Osborn, L.L. Shaw, Int. J. Hydrogen Energy 33 (2008) 3915–3924.
[76] T. Markmaitree, L.L. Shaw, J. Power Sources 195 (2010) 1984–1991.
[77] Z. Xiong, G. Wu, J. Hu, P. Chen, W. Luo, J. Wang, J. Alloys Compd. 417 (2006) 190–194.
[78] J. Hu, Y. Liu, G. Wu, Z. Xiong, P. Chen, J. Phys. Chem.C. 111 (2007) 18439–18443.
[79] C.M. Araújo, R.H. Scheicher, P. Jena, R. Ahuja, Appl. Phys. Lett. 91 (2007) 91924.
[80] Y. Wang, M.Y. Chou, Phys. Rev. B 76 (2007) 14116.
[81] Q. Wang, Y. Chen, J. Gai, C. Wu, M. Tao, J. Phys. Chem. C 112 (2008) 18264–18269.
[82] R. Juza, E. Eberius, Naturwissenschaften 49 (1962) 104.
[83] H. Yamane, T.H. Okabe, O. Ishiyama, Y. Waseda, M. Shimada, J. Alloys Compd. 319 (2001) 124–130.
[84] H.J. Beister, S. Haag, R. Kniep, K. Stroessner, K. Syassen, Angew. Chem. 100 (1988) 1116–1118.
[85] H. Schulz, K. Schwarz, Acta Crystallogr. B 34 (1978) 999–1005.
[86] J. Hu, G. Wu, Y. Liu, Z. Xiong, P. Chen, K. Murata, K. Sakata, G. Wolf, J. Phys. Chem. B 110 (2006) 14688–14692.
[87] O. Reckeweg, F.J. Disalvo, Z. Anorg. Allg. Chem. 627 (2001) 371–377.
[88] R. Juza, F. Hund, Z. Anorg. Allg. Chem. 257 (1948) 1–12.
[89] P. Muthukumar, M. Linder, R. Mertz, E. Laurien, Int. J. Hydrogen Energy 34 (2009) 1873–1879.
[90] Z. Xiong, J. Hu, G. Wu, P. Chen, W. Luo, K. Gross, J. Wang, J. Alloys Compd. 398 (2005) 235–239.
[91] W. Luo, S. Sickafoose, J. Alloys Compd. 407 (2006) 274–281.
[92] W. Luo, E. Rönnebro, J. Alloys Compd. 404–406 (2005) 392–395.
[93] Y. Liu, C. Liang, Z. Wei, Y. Jiang, M. Gao, H. Pan, Q. Wang, Phys. Chem. Chem. Phys. 12 (2010) 3108–3111.
[94] Y. Nakamori, G. Kitahara, K. Miwa, S. Towata, S. Orimo, Appl. Phys. A 80 (2005) 1–3.
[95] A.R. Akbarzadeh, V. Ozoliņš, C. Wolverton, Adv. Mater. 19 (2007) 3233–3239.
[96] T. Ichikawa, K. Tokoyoda, H. Leng, H. Fujii, J. Alloys Compd. 400 (2005) 245–248.
[97] M. Aoki, T. Noritake, Y. Nakamori, S. Towata, S. Orimo, J. Alloys Compd. 446–447 (2007) 328–331.
[98] R. Janot, J.B. Eymery, J.M. Tarascon, J. Power Sources 164 (2007) 496–502.
[99] J.J. Hu, M. Fichtner, Chem. Mater. 21 (2009) 3485–3490.
[100] S.V. Alapati, J.K. Johnson, D.S. Sholl, J. Phys. Chem. B 110 (2006) 8769–8776.
[101] J. Lu, Z.Z. Fang, Y.J. Choi, H.Y. Sohn, J. Phys. Chem. C 111 (2007) 12129–12134.
[102] J. Lu, Y.J. Choi, Z.Z. Fang, H.Y. Sohn, J. Power. Sources 195 (2010) 1992–1997.
[103] W. Osborn, T. Markmaitree, L.L. Shaw, J. Power Sources 172 (2007) 376–378.
[104] Y. Liu, K. Zhong, M. Gao, J. Wang, H. Pan, Q. Wang, Chem. Mater. 20 (2008) 3521–3527.
[105] C. Liang, Y. Liu, K. Luo, B. Li, M. Gao, H. Pan, Q. Wang, Chem. Eur. J. 16 (2010) 693–702.
[106] A. Sudik, J. Yang, D. Halliday, C. Wolverton, J. Phys. Chem. C 111 (2007) 6568–6573.
[107] Y. Chen, P. Wang, C. Liu, H. Cheng, Int. J. Hydrogen Energy 32 (2007) 1262–1268.
[108] Y. Liu, J. Hu, Z. Xiong, G. Wu, P. Chen, J. Mater. Res. 22 (2007) 1339–1345.
[109] Q. Wang, Y. Chen, G. Niu, C. Wu, M. Tao, Ind. Eng. Chem. Res. 48 (2009) 5250–5254.
[110] L. Ma, P. Wang, H. Dai, H. Cheng, J. Alloys Compd. 468 (2009) L21–L24.
[111] L. Ma, Z. Fang, H. Dai, X. Kang, Y. Liang, P. Wang, P. Wang, H. Cheng, J. Mater. Res. 24 (2009) 1936–1942.
[112] L. Ma, H. Dai, Y. Liang, X. Kang, Z. Fang, P. Wang, P. Wang, H. Cheng, J. Phys. Chem. C 112 (2008) 18280–18285.
[113] R.R. Shahi, T.P. Yadav, M.A. Shaz, O.N. Srivastva, Int. J. Hydrogen Energy 35 (2010) 238–246.
[114] J. Wang, Z. Li, H. Li, J. Mi, F. Lv, S. Wang, X. Liu, L. Jiang, Rare Metals 29 (2010) 621–624.
[115] J. Hu, Y. Liu, G. Wu, Z. Xiong, Y.S. Chua, P. Chen, Chem. Mater. 20 (2008) 4398–4402.
[116] J. Hu, E. Weidner, M. Hoelzel, M. Fichtner, Dalton Trans. 39 (2010) 9100–9107.
[117] C. Liang, Y. Liu, Y. Jiang, Z. Wei, M. Gao, H. Pan, Q. Wang, Phys. Chem. Chem. Phys. 13 (2011) 314–321.
[118] X. Zhang, Z. Li, F. Lv, H. Li, J. Mi, S. Wang, Int. J. Hydrogen Energy 35 (2010) 7809–7814.
[119] C. Liang, Y. Liu, Z. Wei, Y. Jiang, F. Wu, M. Gao, H. Pan, Int. J. Hydrogen Energy 36 (2011) 2137–2144.
[120] J. Wang, T. Liu, G. Wu, W. Li, Y. Liu, C.M. Araújo, R.H. Scheicher, A. Blomqvist, R. Ahuja, Z. Xiong, P. Yang, M. Gao, H. Pan, P. Chen, Angew. Chem. Int. Ed. 48 (2009) 5828–5832.
[121] L. Xie, Y. Liu, G. Li, X. Li, J. Phys. Chem. C 113 (2009) 14523–14527.
[122] J. Wang, J. Hu, Y. Liu, Z. Xiong, G. Wu, H. Pan, P. Chen, J. Mater. Chem. 19 (2009) 2141–2146.
[123] P. Chen, Z. Xiong, L. Yang, G. Wu, W. Luo, J. Phys. Chem. B 110 (2006) 14221–14225.
[124] J. Lu, Z.Z. Fang, H.Y. Sohn, Inorg. Chem. 45 (2006) 8749–8754.
[125] W.I.F. David, M.O. Jones, D.H. Gregory, C.M. Jewell, S.R. Johnson, A. Walton, P.P. Edwards, J. Am. Chem. Soc. 129 (2007) 1594–1601.
[126] H. Wu, J. Am. Chem. Soc. 130 (2008) 6515–6522.
[127] H.Y. Leng, T. Ichiwawa, S. Hino, T. Nakagawa, H. Fujii, J. Phys. Chem. B 109 (2005) 10744–10748.
[128] H.Y. Leng, T. Ichiwawa, H. Fujii, J. Phys. Chem. B 110 (2006) 12964–12968.
[129] T. Nakagawa, T. Ichikawa, R. Iida, H.Y. Leng, N. Takeichi, T. Kiyobayashi, H. Takeshita, H. Fujii, J. Alloys Compd. 430 (2007) 217–221.
[130] S. Isobe, T. Ichikawa, H.Y. Leng, H. Fujii, Y. Kojima, J. Phys. Chem. Solids 69 (2008) 2234–2236.
[131] W. Luo, K. Stewart, J. Alloys Compd. 440 (2007) 357–361.
[132] Y. Liu, J. Hu, G. Wu, Z. Xiong, P. Chen, J. Phys. Chem. C 112 (2008) 1293–1298.